JOC Article

Crucial Role of Elusive Isomeric η-Complexes in Gas-Phase Electrophilic Aromatic Alkylations

Enrico Marcantoni,[†] Graziella Roselli,[†] Laura Lucarelli,[†] Gabriele Renzi,[†] Antonello Filippi,[‡] Cristiano Trionfetti,[‡] and Maurizio Speranza*,[‡]

Dipartimento di Scienze Chimiche, Università degli Studi di Camerino, V. S. Agostino 1, I-62032 Camerino (Mc), Italy, and Facoltà di Farmacia, Dipartimento di Studi di Chimica e Tecnologia delle Sostanze Biologicamente Attive (No. 64), Università degli Studi di Roma "La Sapienza", P.le A. Moro 5, I-00185 Roma, Italy

maurizio.speranza@uniroma1.it

Received January 4, 2005

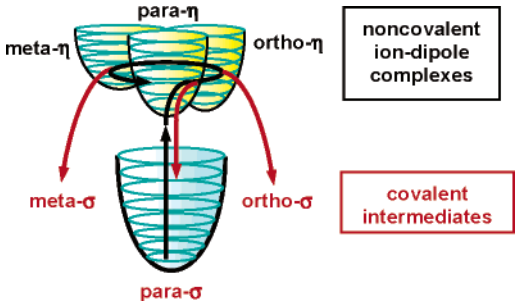

The kinetics and stereochemistry of the protonation-induced unimolecular isomerization of (*R*)-1-D_1-3-(*p*-fluorophenyl)butane have been investigated in the gas phase at 40−100 °C and 70−760 Torr. This process leads to the formation of the relevant *meta* and *ortho* isomers with partial racemization of the migrating *sec*-butyl moiety. Complete racemization is observed, instead, when the isomerization reaction involves a 1,2-H shift in the moving alkyl group. These results, together with the relevant activation parameters, fully confirm the previous evidence of the occurrence in the alkyl cation/arene PES of noncovalent η-type intermediates of defined structure and stability, lying well below the classical π-complexes, as confirmed by ab initio calculations. Their crucial role in determining the positional selectivity of gas-phase electrophilic aromatic substitutions clearly emerges from the comparison of the present results with the site selectivity measured in the corresponding bimolecular arene alkylation carried out at the same temperatures and pressures.

Introduction

Since Dewar's proposal in 1946,[1] the role of the electrostatically bound π-complex in electrophilic aromatic substitutions has been examined thoroughly in both the gaseous[2−20] and condensed phases.[21,22] In the nineties, first Audier's[19] and later Gross' group[19] (A&G) provided convincing mass spectrometric evidence that σ-intermediates from the gas-phase protonation of alkyl-

* To whom correpondence should be addressed. Fax: int. code + (06)49913602.
[†] Università degli Studi di Camerino.
[‡] Università degli Studi di Roma "La Sapienza".

(1) Dewar, M. J. S. *J. Chem. Soc.* **1946**, *406*, 777.
(2) Herman, J. A.; Harrison, A. G. *Org. Mass Spectrom.* **1981**, *16*, 423.
(3) Sen Sharma, D. K.; Ikuta, S.; Kebarle, P. *Can. J. Chem.* **1982**, *60*, 2325.
(4) Grützmacher, H. F.; Filges, U. *Int. J. Mass Spectrom.* **1985**, *64*, 193.
(5) Bäther, W.; Kuck, D.; Grützmacher, H. F. *Org. Mass Spectrom.* **1985**, *20*, 572.
(6) Grützmacher, H. F.; Filges, U. *Org. Mass Spectrom.* **1986**, *21*, 673.
(7) Robin, D.; Prudhomme, P.; Audier, H. E. *Adv. Mass Spectrom.* **1989**, *11a*, 614.
(8) Holman, R. W.; Gross, M. L. *J. Am. Chem. Soc.* **1989**, *111*, 3560.
(9) Audier, H. E.; Monteiro, C.; Morgues, P.; Bartomieu, D. *Org. Mass Spectrom.* **1990**, *25*, 245.
(10) Bartomieu, D.; Audier, H. E.; Monteiro, C.; Denhez, J. P. *Org. Mass Spectrom.* **1991**, *26*, 271.
(11) Bartomieu, D.; Audier, H. E.; Monteiro, C.; Denhez, J. P. *Rapid Commun. Mass Spectrom.* **1991**, *5*, 415.
(12) Bowen, R. D. *Acc. Chem. Res.* **1991**, *24*, 364.
(13) Longevialle, P. *Mass Spectrom. Rev.* **1992**, *11*, 157.
(14) Morton, T. H. *Org. Mass Spectrom.* **1992**, *16*, 423.
(15) Berthomieu, D.; Brenner, V.; Ohanessian, G.; Denhez, J. P.; Millié, P.; Audier, H. E. *J. Phys. Chem.* **1995**, *99*, 712.
(16) Aschi, M.; Troiani, A.; Cacace, F. *Angew. Chem., Int. Ed. Engl.* **1997**, *36*, 83.
(17) Fornarini, S.; Crestoni, M. E. *Acc. Chem. Res.* **1998**, *31*, 827.
(18) Aschi, M.; Attinà, M.; Cacace, F. *Chem.—Eur. J.* **1998**, *4*, 1535.

10.1021/jo050019q CCC: $30.25 © 2005 American Chemical Society
Published on Web 04/19/2005

CHART 1

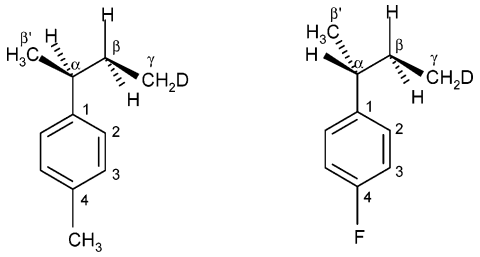

$1^{Me}{}_S$ $1^{F}{}_R$

arenes may coexist with the corresponding electrostatically bonded alkyl cation/arene π-complexes. These findings, coupled with the insight gained from other related work, led A&G to formulate a refined model for gas-phase electrophilic aromatic substitutions whose reaction coordinate may involve the formation of an early π-adduct which eventually collapses to a σ-complex. The actual intermediacy of the π-complex depends on the π-electron density of the aromatic substrate. The larger the π-electron donating ability of the arene, the larger the energy gap between the π-adduct and the more stable σ-complex, and the stronger the tendency of the first to collapse to the latter and to undergo alkyl-group isomerization.

Although the concept of electrostatic complexes as intermediates in electrophilic aromatic substitutions is now consolidated, almost no information is presently available about the mutual orientation of their components and the nature of the forces holding them together. This lack of information is particularly unsatisfactory since, in principle, the structure and dynamics of noncovalent complexes may control their evolution kinetics and the selectivity of the substitution process. One of the first contributions to this crucial theme came from the study of the proton-induced isomerization kinetics of (*S*)-(+)-1-D_1-3-(*p*-tolyl)butane ($\mathbf{1^{Me}_S}$ in Chart 1) in the gas phase at 70 Torr and 100−160 °C.[23] The emerging picture, confirmed by theoretical calculations, suggests that the isomerization may proceed through the intermediacy of low-energy short-lived isomeric η-type structures (lifetime is ca. 10^{-10} s). The presence of the η-type structures encouraged us to reconsider the classical model of gas-phase arene alkylations and allowed us to understand the origin of the marked pressure dependence observed in these reactions when carried out at constant temperatures. Therefore, it would be of extreme interest to verify if the intermediacy of the short-lived η-complexes is restricted to the *sec*-butylation of toluene or if it is a general mechanism for electrophilic aromatic substitutions.

Toward this purpose, we proceeded in the study of the pressure and temperature dependence of the gas-phase proton-induced isomerization of another tailor-made chiral arylalkane, (*R*)-1-D_1-3-(*p*-fluorophenyl)butane ($\mathbf{1^F_R}$ in Chart 1). This compound was chosen because (i) the fluorine substituent has electronic properties largely different than those of the methyl group and (ii) the abnormal *ortho* selectivity exhibited by fluorobenzene in gas-phase alkylations.[24−26] The reaction is carried out in CH_4 at 70 and 760 Torr (T = 40−100 °C) and in the presence of trace amounts of a radical scavenger (O_2) and a powerful base (B = $(C_2H_5)_3N$). $\mathbf{1^F_R}$ was protonated using the strong Brønsted acids, $C_nH_5^+$ (n = 1 or 2), which can conveniently be generated in the gas phase by γ-radiolysis of CH_4.

SCHEME 1

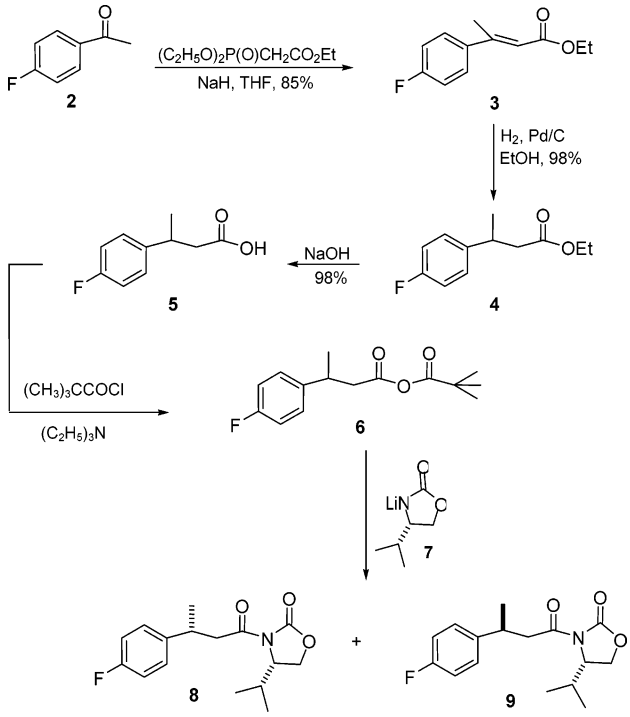

Experimental Section

Synthetic Procedure. The synthesis of the enantiomerically pure (*R*)-1-D_1-3-(*p*-fluorophenyl)butane ($\mathbf{1^F_R}$) started from commercially available *p*-fluoroacetophenone (**2** in Scheme 1) which underwent the Wadsworth−Emmons reaction with a sodium salt of ethyl (diethoxyphosphoryl)acetate[27,28] to produce the α,β-unsaturated ester **3** in an 85% yield. NMR analysis showed that the reaction led almost exclusively to the *E* isomer without any appreciable formation of the *Z* isomer. Catalytic hydrogenation[29] smoothly led to the ester **4** (98% yield) which was subjected to basic hydrolysis with 1 M NaOH at room temperature to produce the pure free acid **5** without side reactions.[30] The racemic 3-(*p*-fluorophenyl)butyric acid (**5**) was then coupled to optically pure (4*S*)-4-isopropyl-1,3-oxazolan-2-one (**7**)[31] via the formation of the mixed anhydride with pivaloyl chloride (intermediate **6**) to yield an almost equimolar mixture of the (4*S*)-4-isopropyl-3-[3-(*p*-fluorophenyl)butanoyl]-

(19) Holman, R. W.; Eary, T.; Whittle, E.; Gross, M. L. *J. Chem. Soc., Perkin Trans. 2* **1998**, 2187.
(20) Kuck, D. *Int. J. Mass Spectrom.* **2002**, *213*, 101.
(21) Olah, G. A. *Acc. Chem. Res.* **1971**, *4*, 240.
(22) Olah, G. A.; Lin, H. C. *J. Am. Chem. Soc.* **1974**, *96*, 2892.
(23) Filippi, A.; Roselli, G.; Renzi, G.; Grandinetti, F.; Speranza, M. *Chem.—Eur. J.* **2003**, *9*, 2072.
(24) Attinà, M.; Giacomello, P. *J. Am. Chem. Soc.* **1979**, *101*, 6040.
(25) Attinà, M.; De Petris, G.; Giacomello, P. *Tetrahedron Lett.* **1982**, *23*, 3525.
(26) Attinà, M.; Ricci, A. *Tetrahedron Lett.* **1991**, *32*, 6775.
(27) Cooke, M. P.; Gopal, D., Jr. *J. Org. Chem.* **1994**, *59*, 260.
(28) Snowden, R. L.; Linder, S. M.; Muller, B. L.; Schulte-Elte, K. H. *Helv. Chim. Acta* **1987**, *70*, 1858.
(29) Durman, J.; Elliott, J.; McElroy, A. B.; Warren, S. *J. Chem. Soc., Perkin Trans. 1* **1985**, 1237.
(30) Hertweck, C.; Moore, B. S. *Tetrahedron* **2000**, *56*, 9115.
(31) Lewis, N.; McKillop, A.; Taylor, R. J. K.; Watson, R. J. *Synth. Commun.* **1995**, *25*, 561.

SCHEME 2

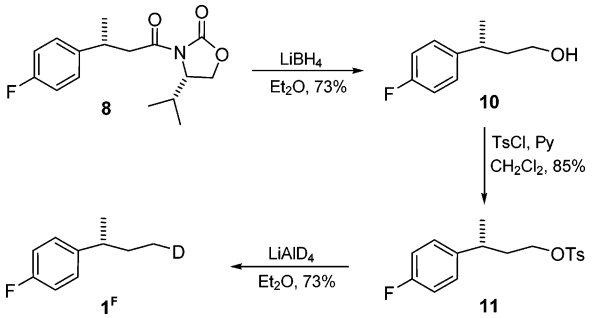

1,3-oxazolan-2-one diastereoisomers **8** and **9**.[32] The relative abundance was determined on the crude material via well-resolved signals in the ^{1}H NMR spectrum. Indeed, since the ^{1}H NMR spectra of these diastereomers are distinctly different,[33] the NMR chemical shift and coupling constant (^3J) of the proton of C(4) of the oxazolidinone ring provide a reliable guide for the assignment of the C(3) configuration of the butyric chain. It should be noted that the use of different substituents at C(4) of oxazolidinone does not permit good assignment of the configuration by NMR spectra. Optically pure stereoisomer **8** was next purified using flash chromatography to produce a 26% yield (based on racemic butyric acid **5**). The chiral auxiliary was subsequently removed using $LiBH_4$ in ether[34] to produce (*R*)-3-(*p*-fluorophenyl)butan-1-ol **10**. The transformation of alcohol **10** into the chiral 1-D_1-3-arylbutane target was achieved by the Kumada method.[35] To this end, alcohol **10** was converted into the related (*R*)-1-D_1-3-(*p*-fluorophenyl)butane ($\mathbf{1^F_R}$) via tosyl ester derivative **11** and substitution with $LiAlD_4$ in ether (Scheme 2).

Most solvents and reagents were used without purification unless otherwise mentioned. Solvents (EtOAc and hexanes) for flash chromatography were distilled. TLC was run on silica gel 60 F_{254} plates (0.25 mm thick) and visualized by UV light, iodine, or a Ce−Mo staining solution (phosphomolybdate, 25 g; $Ce(SO_4)_2{\cdot}2H_2O$, 10 g; concentrated H_2SO_4, 60 mL; water, 940 mL) with heating. Flash chromatography was performed using silica gel 60 (mesh size 0.040−0.063 mm) with a silica gel/crude compound weight ratio of ca. 30:1. Analytical GC was performed with a capillary-fused silica column (0.32 mm × 25 mt), stationary-phase OV1 (film thickness 0.40−0.45 μm). Infrared spectra were taken using thin films on NaCl plates. Only the characteristic peaks are noted. ^{1}H NMR (300 MHz) chemical shifts are reported in parts per million (δ) relative to $CHCl_3$ (7.27 ppm). Coupling constants (*J*) are reported in hertz. ^{13}C NMR spectra were obtained on a 75 MHz spectrometer and are reported in δ relative to $CDCl_3$ (77.2 ppm) as an internal reference. Mass spectra were determined with a gas chromatograph/mass spectrometer (GLC-MS, EI-70 eV). A fused silica column (30 mt × 0.25 mm, cross-linked 5% Ph-Me siloxane, 0.10 μm film thickness) was used with a helium carrier flow rate of 1 mL/min. The temperature of the column was varied, 3 min after the injection, from 65 to 300 °C with a slope of 15 °C min^{-1}.

Ethyl 3-(*p*-Fluorophenyl)-2-butenoate (3). A solution of triethyl phosphonoacetate (7.58 g, 33.8 mmol) in THF (10 mL) was added dropwise within 30 min to a stirred slurry of NaH (0.880 g, 36.68 mmol) in THF (90 mL) at room temperature under nitrogen. During the addition, the temperature rose to 30−35 °C, and after a further 30 min, a solution of 1-(*p*-fluorophenyl)-2-ethanone (**2**) (4 g, 28.96 mmol) in THF (25 mL) was added dropwise within 20 min. The mixture was then refluxed for 24 h and then cooled with a water bath. Then a saturated aqueous ammonium chloride solution (20 mL) was added dropwise to the cold mixture. The aqueous phase was extracted with diethyl ether (4 × 100 mL), and the combined organic phase was washed with brine (3 × 50 mL), dried over sodium sulfate, and concentrated in vacuo. Flash chromatography (95:5 hexanes/ethyl acetate) yielded ester **3** as a clear oil (5.12 g, 85% yield). The product was characterized by IR and GC−MS: IR (thin film) ν = 3050, 2982, 1717, 1631, 1602 cm^{-1}; MS (70 eV, EI) *m/z* (%) 208 (M^+, 46), 179 (30), 163 (100), 133 (70), 115 (50), 109 (44), 96 (17).

Ethyl 3-(*p*-Fluorophenyl)butanoate (4). Unsaturated ester **3** (4.76 g, 22.9 mmol) in absolute ethanol (25 mL) was hydrogenated at 1 atm over 10% palladium on activated carbon (1.724 g) for 15 h. The reaction mixture was filtered through Celite with absolute ethanol as the eluent. The filtrate was evaporated under reduced pressure to produce ester **4** (4.74 g, 98% yield). The GC-MS characterization data were consistent with the target product: MS (70 eV, EI) *m/z* (%) 210 (M^+, 15), 136 (71), 123 (100), 109 (27), 103 (31), 96 (12), 77 (11).

3-(*p*-Fluorophenyl)butanoic Acid (5). Aqueous 1 N sodium hydroxide (150 mL) was added to ester **4** (4.74 g, 22.54 mmol), and the emulsion was stirred overnight at room temperature. The reaction mixture was extracted with diethyl ether, and the ethereal solution was discarded. The aqueous phase was acidified to pH 1 with an aqueous 1 N hydrochloride acid solution and then extracted with diethyl ether (5 × 120 mL). The combined organic extracts were dried over sodium sulfate and concentrated in vacuo to produce pure acid **5** (4.1 g, 82% yield).

(4*S*)-3-[(3*R*)-3-(*p*-Fluorophenyl)butanoyl]-4-isopropyl-1,3-oxazolan-2-one (8). Triethylamine (1.1 mL, 7.88 mmol) and pivaloyl chloride (1 mL, 7.88 mmol) were added to a −78 °C solution of racemic acid **5** (1.35 g, 7.41 mmol) in dry THF (33.2 mL). The resulting white suspension was stirred for 30 min at −78 °C and for 90 min at 0 °C and was cooled to −78 °C. Meanwhile, in a different flask, a solution of metalated oxazolidinone (**7**) was prepared by dropwise addition of *n*-BuLi (1.5 M in hexane, 5.3 mL, 8 mmol) to a −78 °C solution of (4*S*)-4-isopropyl-1,3-oxazolan-2-one (1 g, 7.7 mmol) in dry THF (29 mL), and the mixture was stirred for 30 min at −78 °C. The preformed mixed anhydride **6** was transferred via cannula into the reaction flask containing the lithiated chiral auxiliary at −78 °C. Then, the reaction mixture was stirred at this temperature for 30 min, and after being allowed to warm to room temperature overnight, the mixture was quenched with saturated ammonium chloride solution (20 mL) and THF and evaporated in vacuo. The mixture was diluted with methylene chloride (300 mL) and washed with saturated sodium hydrogen carbonate (2 × 30 mL), water (2 × 30 mL), and brine (30 mL). The organic phase was dried over sodium sulfate and concentrated in vacuo. Flash chromatography on a silica gel column (6:3.5:0.5 hexanes/benzene/ethyl acetate) produced optically pure **8** as a white solid (0.549 g, 26% yield): ^{1}H NMR (300 MHz, $CDCl_3$) δ = 7.35−7.19 (m, 2H), 7.00−6.92 (m, 2H), 4.41−4.35 (m, 1H), 4.26−4.11 (m, 2H), 3.57−3.32 (m, 2H), 2.94 (dd, *J* = 15.02 and 6.23 Hz, 1H), 2.18−2.11 (m, 1H), 1.30 (d, *J* = 6.96 Hz, 3H), 0.82 (d, *J* = 6.96 Hz, 3H), 0.66 (d, *J* = 6.96 Hz, 3H); ^{13}C NMR (75 MHz, $CDCl_3$) δ = 14.5, 18.0, 22.3, 28.5, 35.8, 43.3, 58.5, 63.4, 115.2, 115.5, 128.6, 128.7, 141.5, 154.2, 160.0, 163.3, 171.9; MS (70 eV, EI) *m/z* (%) 293 (M^+, 13), 278 (7), 149 (15), 136 (100), 123 (98), 109 (27), 103 (37), 77 (13), 55 (4), 41 (21). Elemental analysis calcd (%) for $C_{16}H_{20}FNO_3$ (293.14): C, 65.51; H, 6.87; N, 4.78. Found: C, 65.45; H, 6.27; N, 4.32.

(3*R*)-3-(*p*-Fluorophenyl)butan-1-ol (10). The acyloxazolidinone **8** (0.53 g, 1.87 mmol) was stirred in dry ethyl ether (38 mL) under nitrogen. Water (37.4 μL, 2.06 mmol) was added, and the reaction mixture was cooled to 0 °C in an ice bath. Lithium borohydride (1.03 mL, 2.06 mmol) was added dropwise causing immediate clouding and hydrogen evolution.

(32) Li, G.; Patel, D.; Hruby, V. J. *J. Chem. Soc., Perkin Trans. 1* **1994**, 3057.
(33) Dharanipragada, R.; VanHulle, K.; Bannister, A.; Bear, S.; Kennedy, L.; Hruby, V. J. *Tetrahedron* **1992**, *48*, 4733.
(34) Penning, T. D.; Djuric, S. W.; Haack, R. A.; Kalish, V. J.; Miyashiro, J. M.; Rowell, B. W.; Yu, S. S. *Synth. Commun.* **1990**, *20*, 307.
(35) Hayashi, T.; Konishi, M.; Fukushima, M.; Mise, T.; Kagotani, M.; Tajika, M.; Kumada, M. *J. Am. Chem. Soc.* **1982**, *104*, 180.

The mixture was allowed to warm to room temperature and was stirred for 3 h at this temperature. The reaction was then quenched with an aqueous sodium hydroxide solution (1 M, 40 mL), and the mixture was stirred until both layers were clear. The mixture was extracted with diethyl ether (5 × 80 mL), and the organic phase was washed with water (2 × 20 mL) and brine (20 mL), dried over sodium sulfate, and concentrated in vacuo. Flash chromatography (3.5:6.5 hexanes/ethyl acetate) produced primary alcohol **10** (0.28 g, 90% yield) along with the recovered chiral auxiliary. The product was characterized by IR and ^{1}H NMR: IR (thin film) $\acute{\nu}$ = 3400, 2957, 1641, 1219 cm^{-1}; ^{1}H NMR (300 MHz, $CDCl_3$) δ = 7.20−7.11 (m, 2H), 7.04−6.94 (m, 2H), 3.55 (dt, J = 6.85 and 6.32 Hz, 2H), 2.88 (bs, OH, 1H), 2.50−2.57 (m, 1H), 1.64−1.72 (m, 2H), 1.20 (d, J = 7.02 Hz, 3H). Elemental analysis calcd (%) for $C_{10}H_{13}FO$ (168.21): C, 71.40; H, 7.79. Found C, 71.45; H, 7.27.

(3*R*)-3-(*p*-Fluorophenyl)butyl 4-Methyl-1-benzenesulfonate (11). A solution of alcohol **10** (0.154 g, 0.916 mmol) in dichloromethane (2 mL) was treated with tosyl chloride (0.22 g, 1.16 mmol) and pyridine (97 μL, 1.21 mmol) and stirred at room temperature for 5 h. The reaction mixture was then diluted with diethyl ether (100 mL) and washed with a 5% aqueous hydrochloride solution (3 × 25 mL). The organic phase was washed with a saturated aqueous sodium hydrogen carbonate solution (2 × 20 mL) and brine (2 × 15 mL), dried over sodium sulfate, and concentrated in vacuo. Flash chromatography (9:1 hexanes/ethyl acetate) produced **11** as a pale yellow oil (0.26 g, 85% yield). The product was characterized by GC−MS: MS (70 eV, EI) *m/z* (%) 322 (M^+, 19), 150 (63), 135 (100), 123 (51), 109 (31), 91 (47), 103 (37), 77 (11), 65 (21).

(3*R*)-1-D$_1$-3-(*p*-Fluorophenyl)butane ($\mathbf{1^F_R}$). An ether solution (5 mL) of the tosylate **11** (0.224 g, 0.694 mmol) was added to a suspension of lithium aluminum deuteride (33.2 mg, 0.79 mmol) in ether (7 mL) at 0 °C with an ice bath. The reaction mixture was stirred at room temperature for 10 min and then refluxed for 5 h. After hydrolysis by successive addition of (i) water (0.03 mL), (ii) 15% aqueous sodium hydroxide solution (0.03 mL), and (iii) water (0.09 mL), the precipitate formed was eventually filtered off. The filtrate (180 mL) was washed with a saturated aqueous sodium hydrogen carbonate solution (2 × 25 mL) and brine (2 × 25 mL) and dried over magnesium sulfate. The solvent was removed in vacuo. Flash chromatography on a silica gel column (1:1 diethyl ether/petroleum ether) produced the target product, $\mathbf{1^F_R}$ (57 mg, 73% yield). The product was characterized by GC−MS: MS (70 eV, EI) *m/z* (%) 153 (M^+, 23), 123 (100), 109 (27), 103 (39), 96 (9), 77 (11), 51 (4).

Radiolytic Procedure. Methane, *n*-butane, fluorobenzene, oxygen, and triethylamine were commercially available high-purity compounds used without further purification. The gaseous mixtures were prepared by conventional procedures with the use of a greaseless vacuum line. Two sets of experiments were carried out. In the first series, the starting chiral arene, $\mathbf{1^F_R}$, the thermal radical scavenger, O_2, and the base, $(C_2H_5)_3N$ (proton affinity (PA) = 234.7 kcal mol^{-1}),[36] were introduced into carefully outgassed 130 mL Pyrex bulbs, each equipped with a break-seal tip. The bulbs were filled with CH_4 (60 or 750 Torr), cooled to liquid-nitrogen temperature, and sealed off. In the second set of experiments, the gaseous mixtures were prepared containing traces of fluorobenzene **16**, O_2, $(C_2H_5)_3N$, and butane (60 or 750 Torr), cooled to liquid-nitrogen temperature, and sealed off. The gaseous mixtures were submitted to irradiation at a constant temperature (40−100 °C) in a ^{60}Co γ-source (dose 2 × 10^4 Gy, dose rate 1 × 10^3 Gy h^{-1}, determined with a neopentane dosimeter). Control experiments, carried out at doses ranging from 1 × 10^4 to 1 × 10^5 Gy, showed that the relative yields of products are largely independent of the dose. The radiolytic products were analyzed by GLC-MS. The following chiral columns were used: (i) a 25 m long, i.d. 0.25 mm i.d., d_f = 0.25 μm MEGADEX 5 column operated at 40 < T < 170 °C, 4 °C min^{-1}; (ii) a 25 m long, 0.25 i.d., d_f = 0.25 μm CP-Chirasil-DEX CB column operated at 40 < T < 170 °C, 4 °C min^{-1}; and (iii) a 25 m long, 0.25 i.d., d_f = 0.25 μm Dimethylpentyl β-CDX (PS 086) column operated at 40 < T < 170 °C, 4 °C min^{-1}. The yields of the radiolytic products were determined from the areas of the corresponding eluted peaks using an internal standard (acetophenone) and individual calibration factors to correct for the detector response. Control experiments were performed to rule out the occurrence of thermal fragmentation, isomerization, and racemization of the starting arene as well as of their isomeric products within the temperature range investigated.

The D-content and location in the radiolytic products from the first set of experiments were determined by GLC-MS; the mass analyzer was set in the selected ion mode (SIM). The ion fragments at *m/z* 123 ($[M - C_2H_4D]^+$), 124 ($[M - C_2H_5]^+$), and 153 ($[M]^{\bullet+}$) were monitored to analyze all of the GLC-separated isomers of $\mathbf{1^F_R}$ (=M). Fluorobenzene **16**, obtained from $\mathbf{1^F_R}$, was analyzed by monitoring its parent ion at *m/z* 96.

Computational Details. Quantum-chemical ab initio calculations were performed using the Unix version of the Gaussian 98 program.[37] The geometries of the investigated species have been optimized, by analytical-gradient techniques, at the HF/6-31+G** level of theory, and the located critical points have been unambiguously characterized as true minima on the potential energy surface by computing, at the same computational level, the corresponding analytical vibrational frequencies. The latter values were used to calculate the zero-point vibrational energies (ZPE).

Results

Radiolytic Experiments. Table 1 shows the composition of the irradiated systems as well as the identity and the yields (Y_i) of the major products, i.e., (±)-1-D$_1$-3-(*m*-fluorophenyl)butane (**12**), (±)-1-D$_1$-2-(*m*-fluorophenyl)-butane (**13**), (±)-1-D$_1$-3-(*o*-fluorophenyl)butane (**14**), (±)-1-D$_1$-2-(*o*-fluorophenyl)butane (**15**), and fluorobenzene (**16**), obtained from gas-phase $C_nH_5^+$ (n = 1 or 2) protonation of $\mathbf{1^F_R}$ in the presence of trace amounts of $(C_2H_5)_3N$ (0.1 Torr) (Scheme 3). The table does not include other minor products, i.e., isomeric (±)-1-D$_1$-3-(tolyl)butanes, which arise from the well-known addition to the methane bulk gas of *para sec*-butylphenyl cations, generated by $C_nH_5^+$ (n = 1 or 2)-induced defluorination of $\mathbf{1^F_R}$.[38] It should be noted that, despite a specific search, no appreciable amounts of (*S*)-1-D$_1$-3-(*p*-fluorophenyl)butane or (*S*)-1-D$_1$-2-(*p*-fluorophenyl)butane were detected among the products.

The numbers in the table represent average values obtained from several separate irradiations carried out under the same experimental conditions, and their reproducibility is expressed by the uncertainty level

(36) National Institute of Standards and Technology (NIST)-USA, http://webbook.nist.gov/chemistry/.

(37) Frish, M. J.; Trucks, G. W.; Schlegel, H. B.; Scuseria, G. E.; Robb, M. A.; Cheeseman, J. R.; Zakrzewski, V. G.; Montgomery, J. A.; Stratman, R. E., Jr.; Burant, J. C.; Dapprich, S.; Millam, J. M.; Daniels, A. D.; Kudin, K. N.; Strain, M. C.; Farkas, O.; Tomasi, J.; Barone, V.; Cossi, M.; Cammi, R.; Mennucci, B.; Pomelli, C.; Adamo, C.; Clifford, S.; Ochterski, J.; Petersson, G. A.; Ayala, P. Y.; Cui, Q.; Morokuma, K.; Malik, D. K.; Rabuck, A. D.; Raghavachari, K.; Foresman, J. B.; Cioslowski, J.; Ortiz, J. V.; Raboul, A. G.; Stefaniv, B. B.; Liu, G.; Liashenko, A.; Piskorz, P.; Nanayakkara, I.; Gonzales, C.; Challacombe, M.; Gill, P. M. W.; Johnson, B.; Chen, W.; Wong, M. W.; Andres, J. L.; Gonzales, C.; Head-Gordon, M.; Replogle, E. S.; Pople, J. A. *Gaussian 98*, revision A7; Gaussian, Inc.: Pittsburgh, PA, 1998.

(38) Speranza, M.; Cacace, F. *J. Am. Chem. Soc.* **1977**, *99*, 3051.

TABLE 1. Kinetics of Gas-Phase Isomerization and Dealkylation of Protonated (*R*)-(+)-1-D-3-(*p*-Fluorophenyl)butane 1^F_R

syst comp[a] (Torr) 1^F_R	rxn temp (°C)	rxn time (τ) ($\times 10^7$ s)[b]	Y_{12}[c]	Y_{13}[c]	Y_{14}[c]	Y_{15}[c]	Y_{16}[c]	Σ[d]	k_{12}[e] ($\times 10^{-5}$ s^{-1})	k_{13}[e] ($\times 10^{-5}$ s^{-1})	k_{14}[e] ($\times 10^{-5}$ s^{-1})	k_{15}[e] ($\times 10^{-5}$ s^{-1})	k_{16}[e] ($\times 10^{-5}$ s^{-1})
0.30	40	1.14	0.56	0.50	0.42	0.48	5.07	7.03	0.50 (4.70)	0.46 (4.66)	0.39 (4.59)	0.43 (4.64)	4.61 (5.66)
0.29	60	1.40	1.60	0.99	1.08	0.96	12.28	16.91	1.25 (5.10)	0.77 (4.89)	0.84 (4.93)	0.75 (4.87)	5.95 (5.98)
0.39	70	1.22	2.46	1.51	2.39	1.96	16.92	25.24	2.31 (5.36)	1.41 (5.15)	2.26 (5.35)	1.84 (5.27)	15.94 (6.20)
0.16	90	1.27	3.80	2.23	3.84	2.90	26.94	39.71	3.82 (5.58)	2.24 (5.35)	3.86 (5.59)	2.91 (5.46)	27.07 (6.43)
0.36	100	1.90	8.24	4.06	7.00	5.07	29.79	54.16	5.83 (5.79)	3.08 (5.49)	5.29 (5.72)	3.84 (5.58)	22.53 (6.35)

[a] CH_4, 60 Torr; O_2, 10 Torr; $(C_2H_5)_3N$, 0.1 Torr; radiation dose, 2×10^4 Gy (dose rate 1×10^4 Gy h^{-1}). [b] Reaction time, τ, calculated from the reciprocal of the first-order collision constant between the relevant ionic adduct and $(C_2H_5)_3N$ (see text). [c] $Y = 100[G(\text{product})/G(C_nH_5^+)]$ (G values expressed as the number of molecules of the given species per 100 eV of energy absorbed by the gaseous mixture). The percent distribution of products is in parentheses. [d] $\Sigma = Y_{(\pm)\text{-}\mathbf{12}} + Y_{(\pm)\text{-}\mathbf{13}} + Y_{(\pm)\text{-}\mathbf{14}} + Y_{(\pm)\text{-}\mathbf{15}} + Y_{\mathbf{16}}$. Each value is the average of several determinations, with an uncertainty level of ca. 5%. [e] Log k in parentheses.

TABLE 2. Retention vs Inversion of Configuration in the Gas-Phase Isomerization of Protonated (*R*)-(+)-1-D-3-(*p*-Fluorophenyl)butane 1^F_R at 70 Torr[a]

syst comp[a] 1^F_R (Torr)	rxn temp (°C)	**12** (*ret/inv*)	**13** (*ret/inv*)	**14** (*ret/inv*)	**15** (*ret/inv*)	(**14**+**15**)/(**12**+**13**) (*ortho/meta*)
0.30 (0.35)	40	1.44 (1.50)	1.17 (1.08)	2.33 (1.13)	0.85 (1.04)	0.85 (1.38)
0.29 (0.32)	60	1.86 (1.38)	1.04 (1.17)	1.27 (1.27)	0.89 (1.00)	0.79 (1.00)
0.39 (0.19)	70	1.78 (2.03)	1.04 (0.82)	1.50 (1.04)	0.96 (0.82)	1.10 (1.50)
0.16 (0.19)	90	1.86 (1.70)	1.00 (1.00)	1.44 (1.38)	1.00 (0.96)	1.12 (1.50)
0.36 (0.35)	100	2.12 (2.57)	1.04 (1.04)	1.70 (1.27)	1.00 (0.89)	0.98 (1.50)

[a] Values in parentheses refer to experiments carried out at CH_4, 750 Torr; O_2, 10 Torr; $(C_2H_5)_3N$, 0.1 Torr; radiation dose, 2×10^4 Gy (dose rate 1×10^4 Gy h^{-1}).

SCHEME 3

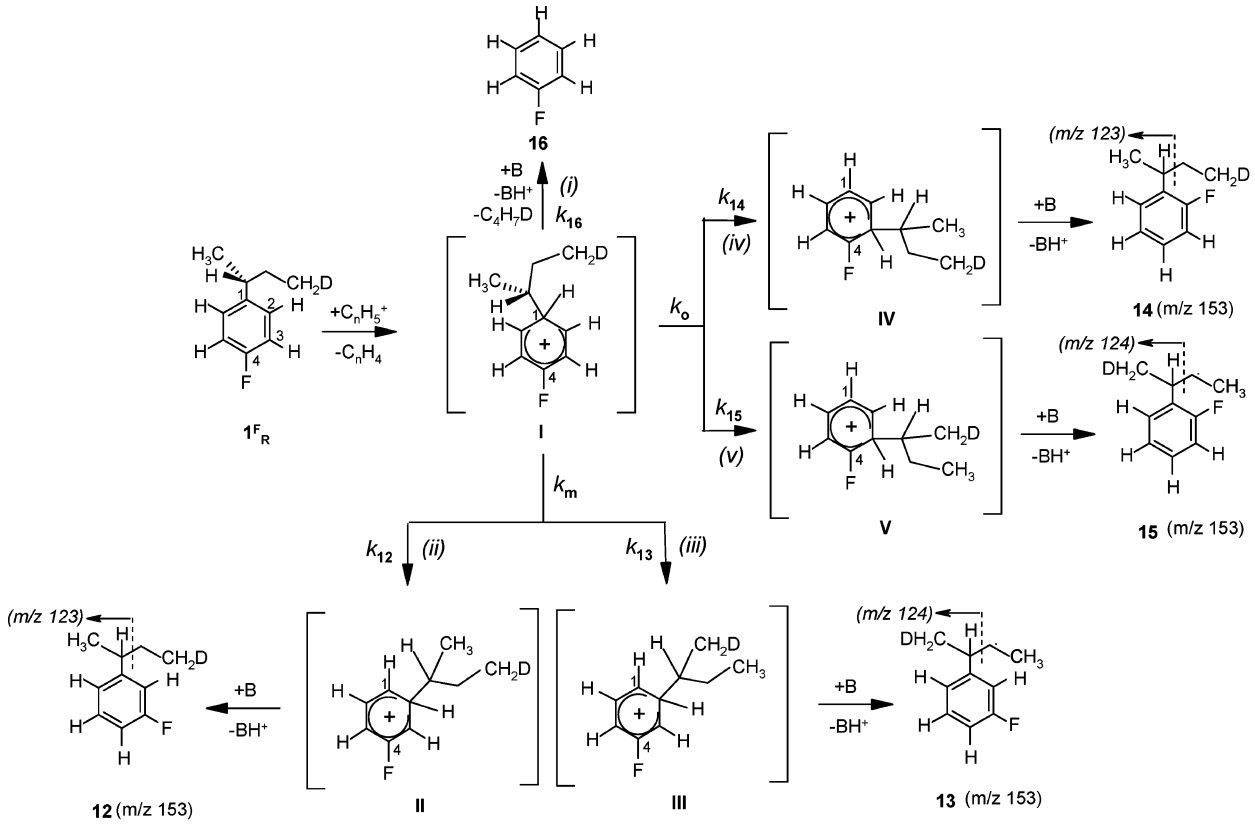

quoted. The ionic origin of the radiolytic products is demonstrated by the sharp decrease (more than 80%) of their abundance as the $(C_2H_5)_3N$ concentration is raised from ca. 0.1 to ca. 0.5 mol %.

The enantiomeric distribution of products **12**−**15** (*ret/inv*) is given in Table 2. The observed product pattern results from the isomerization of the *ipso*-protonated intermediate **I** of Scheme 3, while fluorobenzene **16** derives from its de-*sec*-butylation. The long-recognized reluctance of the aromatic fluorine to migrate around the aromatic ring[39] coupled with the extensive racemization and the side-chain H-shift, observed in the isomer-

(39) Cacace, F.; Speranza, M. *J. Am. Chem. Soc.* **1976**, *98*, 7305.

TABLE 3. Arrhenius Parameters for the Gas-Phase Isomerization and Dealkylation of I

process	Arrhenius equation ($y = 1000/2.303RT$)	corr coeff (r^2)	ΔH^* (kcal mol^{-1})	ΔS^* (cal mol^{-1} K^{-1})
I → II	$\log k_{12} = (11.4 \pm 0.3) - (9.5 \pm 0.5)y$	0.990	8.9 ± 0.6	−8.4 ± 1.6
I → III	$\log k_{13} = (9.9 \pm 0.4) - (7.5 \pm 0.6)y$	0.983	6.9 ± 0.9	−15.2 ± 1.7
I → IV	$\log k_{14} = (11.8 \pm 0.7) - (10.4 \pm 1.1)y$	0.969	9.8 ± 1.1	−6.2 ± 3.1
I → V	$\log k_{15} = (10.7 \pm 0.7) - (8.8 \pm 1.0)y$	0.959	8.2 ± 1.0	−11.3 ± 3.1
I → 16	$\log k_{16} = (12.0 \pm 0.6) - (6.4 \pm 1.3)y$	0.893	6.5 ± 1.2	−12.0 ± 3.6

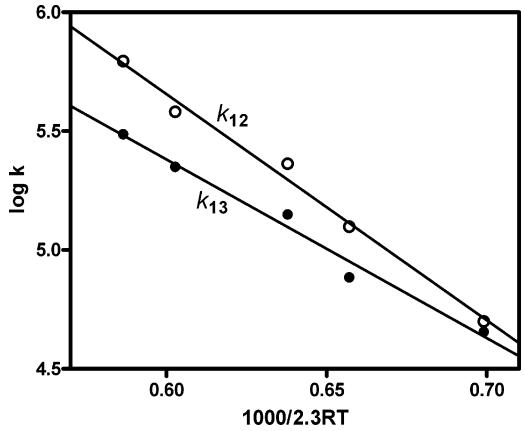

FIGURE 1. Temperature dependence of the k_{12} (○) and k_{13} (●) rate constants for the **I** → **II** and **I** → **III** reactions, respectively.

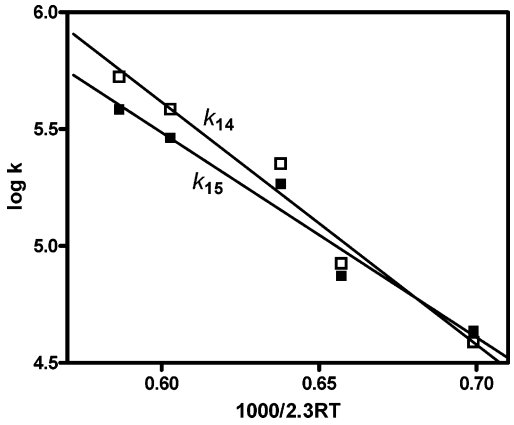

FIGURE 2. Temperature dependence of the k_{14} (□) and k_{15} (■) rate constants for the **I** → **IV** and **I** → **V** reactions, respectively.

ization products, rules out any alternative isomerization pathways.

According to Scheme 3, and with the assumption that the $C_nH_5^+$ protonation of $\mathbf{1^F_R}$ leads predominantly to the products of Table 1 and that the deprotonation of the relevant ionic precursor by $(C_2H_5)_3N$ is fast, the rate constants for de-*sec*-butylation of **I** (k_{16}), its isomerization without side-chain rearrangement (k_{12} and k_{14}), and its isomerization with side-chain rearrangement (k_{13} and k_{15}) can be calculated by inserting the appropriate Y_i values in eq 1, where Y_i (=100 × [$G_i/G(C_nH_5^+)$])[40] is the absolute percent yield of the *i*th product relative to the starting **I**, $\sum = Y_{12} + Y_{13} + Y_{14} + Y_{15} + Y_{16}$, and τ is the collision time between the arenium ions and B = $(C_2H_5)_3N$ ($\tau = (k_{coll}[B])^{-1}$) at the given temperature.[41]

$$k_i = \frac{Y_i \ln[100/(100 - \sum)]}{\tau \sum} \qquad (1)$$

The Arrhenius plots of k_{12} and k_{13} over the 40−100 °C temperature range are reported in Figure 1. Figure 2 illustrates the Arrhenius plots of k_{14} and k_{15} over the same temperature range. A similar linear plot is obtained for the de-*sec*-butylation of **I** under the same conditions (k_{16}). The relevant linear curves obey the equations listed in Table 3, which also shows the corresponding activation parameters, as calculated from the transition state theory.

Ancillary experiments were carried out to shed some light on the specific mechanism of the isomerization of **I**. Thus, the ionic *sec*-butylation of fluorobenzene was carried out at temperatures from 40 to 100 °C using free *sec*-butyl cations generated by the γ-radiolysis of butane (70−760 Torr). At any temperature, 2-(*o*-fluorophenyl)-butane is the dominant product which is accompanied by minor amounts of the *para* and *meta* regioisomers (Table 4). The abundance of these latter products increases when the pressure decreases and temperature increases, in agreement with the behavior of strictly related gas-phase electrophilic alkylations on the same substrate.[24−26] The striking difference in the [2-(*o*-fluorophenyl)butane]/[2-(*m*-fluorophenyl)butane] yield ratio from the *sec*-butylation of fluorobenzene (*ortho*/*meta*: 2.0 (40 °C); 1.5 (100 °C); Table 4) and that obtained from **I** isomerization under the same conditions (*ortho*/*meta*: 0.8 (40 °C); 1.0 (100 °C); Table 1) excludes the possibility that the two reactions proceed through the intermediacy of the same loosely bound alkyl cation/arene π-complexes.

TABLE 4. Isomeric Distribution of 2-(Fluorophenyl)butanes from the Gas-Phase *sec*-Butylation of Fluorobenzene[a]

syst comp **16** (Torr)	*n*-butane (Torr)	rxn temp (°C)	*ortho* (%)	*meta* (%)	*para* (%)	*ortho*/*meta*	overall $G_{(M)}$
0.99	70	40	43	21	36	2.05	3.69
0.74	70	100	45	29	26	1.55	2.89
0.70	400	40	72	5	23	14.40	0.53
0.83	760	40	76	4	20	19.00	0.95
0.79	760	70	68	6	26	11.33	1.26
0.77	760	100	55	11	34	5.00	0.32

[a] O_2, 10 Torr; $(C_2H_5)_3N$, 0.1 Torr; radiation dose, 2 × 10^4 Gy (dose rate 1 × 10^4 Gy h^{-1}).

Theoretical Calculations. The stable intermediates and transition structures involved in **I** isomerization were investigated by quantum-chemical ab initio calculations at the HF/6-31+G** level of theory. The exploration of the potential energy surface (PES) of **I** around conceiv-

(40) *G* values are expressed as the number of molecules produced per 100 eV of energy absorbed by the gaseous mixture. $G(C_nH_5^+)$ = 1.9 (n = 1), 0.9 (n = 2). See: Ausloos, P.; Lias, S. G.; Gorden, R., Jr. *J. Chem. Phys.* **1963**, *39*, 3341.

(41) The collision constant, k_{coll}, between the arenium ions of Scheme 3 and $(C_2H_5)_3N$ is calculated according to the following: Su, T.; Chesnavitch, W. J. *J. Chem. Phys.* **1982**, *76*, 5183.

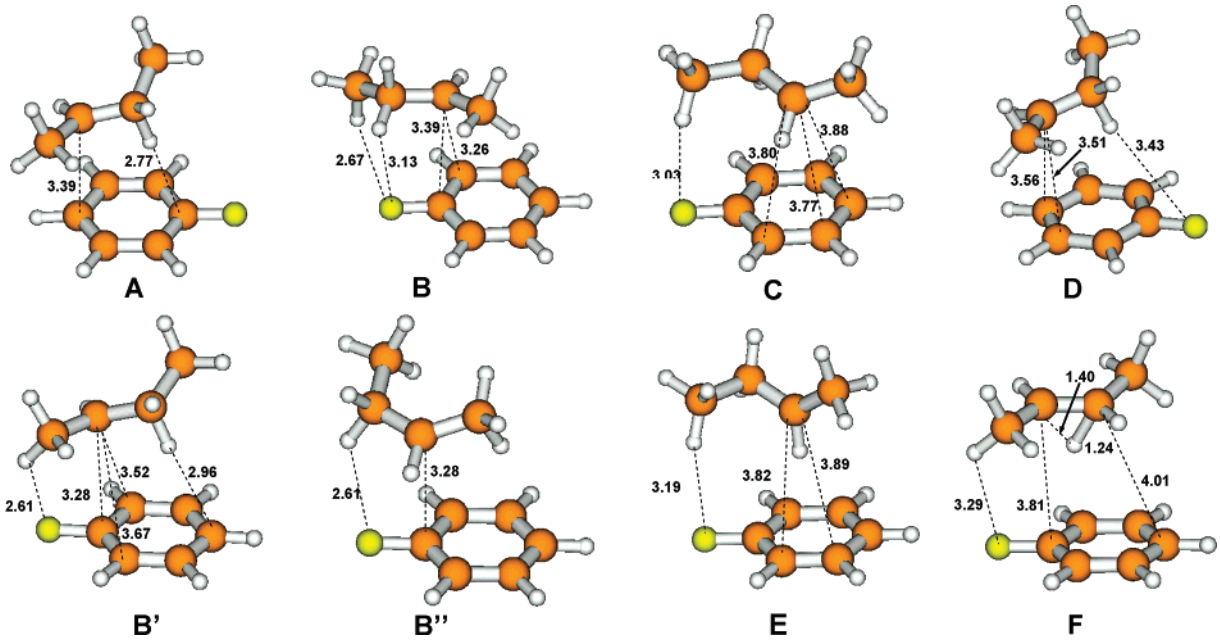

FIGURE 3. Geometrical parameters of the main HF/6-31+G**-optimized critical structures located on the potential energy surface (PES) of **I** (bond lengths in Å). See also Supporting Information for structures **I**–**V** and for computational details.

able regions led to the location of several distinct critical structures which were unambiguously characterized as true minima or first-order saddle points by analytical computation of the corresponding vibrational frequencies. The connectivity and the main geometrical parameters of these structures are shown in Figure 3.

Discussion

Energetics. Gas-phase protonation of $\mathbf{1^F_R}$ by the strong Brønsted acids, $C_nH_5^+$ ($n = 1$ or 2), is an exothermic process yielding the corresponding arenium ion protomers. Formation of the *ipso*-protonated intermediate **I** is estimated to be exothermic by 53 ($n = 1$) and 20 kcal mol^{-1} ($n = 2$).[42] The excess energy imparted to ion **I** and the C_nH_4 fragments by the exothermicity of their formation process is efficiently dissipated by multiple unreactive collisions with the bulk CH_4 gas. As illustrated in Scheme 3, *ipso*-intermediate **I** isomerizes to the *meta* and *ortho* structures **II** and **IV**, respectively, with no H-scrambling and partial racemization of the *sec*-butyl group (Table 2), or to the *meta* and *ortho* structures **III** and **V**, respectively, with complete rearrangement and racemization of the *sec*-butyl group (Table 2). Alternatively, *ipso*-intermediate **I** can undergo de-*sec*-butylation to eventually produce fluorobenzene **16** (Table 1).

With the reasonable assumption that the proton affinity (PA) of $\mathbf{1^F_R}$ at C(1) is comparable to that of *p*-fluorotoluene (PA = 182.6 kcal mol^{-1}),[42] the heat of formation of **I** can be estimated as 132 kcal mol^{-1}. According to HF/6-31+G** calculations, the heat of formation of **II** (and **III**) can be estimated as 140 kcal mol^{-1}, whereas that of **IV** (and **V**) is ca. 135 kcal mol^{-1}.[43] Unimolecular dissociation of **I** to produce either the separated fluorobenzene/*sec*-butyl cation or the *p*-fluorobenzenium ion/2-butene pairs can be calculated to be ca.

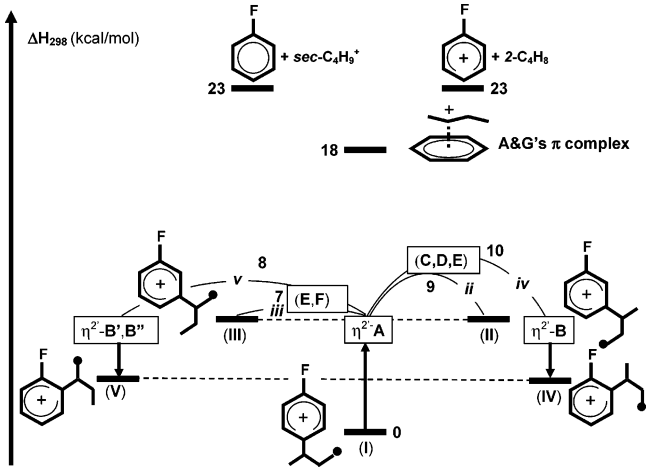

FIGURE 4. Schematic potential energy reaction coordinate diagram for the gas-phase *sec*-butylation of fluorobenzene.

23 kcal mol^{-1} endothermic (Figure 4), in good agreement with previous calculations carried out at the AM1 semiempirical level.[19]

The Isomerization and Dealkylation Reactions. As pointed out above, the formation of 1-D_1-3-(*m*-fluorophenyl)butane (**12**) from $\mathbf{1^F_R}$ must be the result of the **I** → **II** isomerization (path (ii) in Scheme 3) involving the partial racemization of the chiral *sec*-butyl moiety (Table 2). This isomerization process is accompanied by a **I** → **IV** isomerization (path (iv) in Scheme 3), almost as extensive as the **I** → **II** isomerization, leading to a

(42) Hunter, E. P.; Lias, S. G. *J. Phys. Chem. Ref. Data* **1998**, *27*, 413.

(43) According to ref 42, the proton affinity of the *para* position of fluorobenzene is identical to that of *p*-fluoro-*tert*-butylbenzene at C(1) (PA = 182.6 kcal mol^{-1}). It is therefore plausible to take the same proton affinity for the C(1) center of *p*-fluoro-*sec*-butylbenzene. Given the vanishingly small effect of the alkyl group on the PA of fluoroalkylbenzenes at the C-alkyl site, the PA of isomeric fluoro-*sec*-butylbenzenes is taken to be equal to that of the corresponding *ortho*, *meta*, and *para* positions of fluorobenzene.

partially racemized 1-D_1-3-(*o*-fluorophenyl)butane (**14**). The good linearity of the relevant Arrhenius plots (Figures 1 and 2) supports the view that isomerization processes (ii) and (iv) proceed independently without any appreciable **II** ↔ **IV** interconversion. Similarly independent reactions involve a 1,2-H shift in the moving *sec*-butyl moiety, i.e., **I** → **III** and **I** → **V** (paths (iii) and (v) in Scheme 3, respectively). They lead to completely racemized (±)-1-D_1-2-(*m*-fluorophenyl)butane (**13**) and (±)-1-D_1-2-(*o*-fluorophenyl)butane (**15**), respectively. It may be argued, in this case, that the partial racemization observed in the formation of **12** and **14** from **I** is to be ascribed to a fast reversible 1,2-H shift in the moving *sec*-butyl moiety. This process would lead to the formation of [(±)-**12**]/[(±)-**13**] = [(±)-**14**]/[(±)-**15**] = ca. 1 and, therefore, contribute to the racemization of **12** and **14**. However, a fast reversible 1,2-H shift in the side chain of **I** is also expected to produce appreciable amounts of both (*S*)-1-D_1-3-(*p*-fluorophenyl)butane and (*S*)-1-D_1-2-(*p*-fluorophenyl)butane which instead are completely absent from the products. On these grounds, it is concluded that the formation of **13** and **15** proceeds through just a single irreversible 1,2-H shift in the side chain of **I** leading to transient species which rapidly convert to the corresponding *σ*-bonded intermediates.

The incomplete *sec*-butyl group racemization in the **I** → **II** and **I** → **IV** reactions points to transition structures in which the C(1)−C(α) bond (Chart 1) is sufficiently elongated to allow positional shifting of the *sec*-butyl moiety but not so elongated to allow full rotation around its C(α)−C(*β*) bond.[8,15,44] Exploration of the PES governing the **I** → **II** and **I** → **IV** reactions led to the location of several distinct critical points, identified as true minima (i.e., **A** and **B** of Figure 3) and as transition structures (i.e., **C**, **D**, and **E** of Figure 3).

The first consideration is the nature of the quasi-degenerate intermediates **A** and **B**. The geometry of complex **A** reflects specific C(α)···C(1) (3.39 Å) and C(*β*)-H···C(4) (2.77 Å) electrostatic interactions. Simple sliding of the *sec*-butyl group in **A** over the aromatic ring leads to intermediate **B**. This complex presents C(*γ*)-H···F (2.67 Å) and C(*β*)-H···F (3.13 Å) hydrogen bonds coupled with a C(α)···C(3) interaction (3.26 Å) which is suitably predisposed for *σ*-bonding to the more stable intermediate, **IV** (path (iv) in Figure 4). The arrangements of the specific noncovalent forces in **A** and **B** do not allow us to classify them into the well-established η^1- and η^2-categories,[45] and therefore, we coined the symbol $\eta^{2'}$ to denote the chelating interactions operating in these noncovalent structures. In competition with the **A** → **B** motion, the *sec*-butyl group in $\eta^{2'}$-chelate **A** may slide over the adjacent *meta* positions eventually yielding *σ*-intermediate **II**. Since it takes place without any C(α)−C(*β*) bond rotation, the **A** → **II** process may involve two different although almost degenerate transition structures, i.e., **C** and **D** of Figure 3 (path (ii) in Figure 4). Besides the **A** → **B** and **A** → **II** sliding, $\eta^{2'}$ chelate **A** can undergo C(α)−C(*β*) bond rotation through transition structure **E** of Figure 3. It is interesting to note that the formerly empty p orbital of the *sec*-butyl moiety in **E** simultaneously faces both the C(2) and C(5) ring atoms thus pointing to a facile *meta* ↔ *ortho′* isomerization, when allowed by the experimental conditions.

The activation parameters measured for the **I** → **IV** isomerization (iv) ($\Delta H^{\ddagger} = 9.8 \pm 1.1$ kcal mol^{-1} and $\Delta S^{\ddagger} = -6.2 \pm 3.1$ cal mol^{-1} K^{-1}) conform to a **I** → **B** transition structure in which the C(α)$^+$···C(1) interaction is sufficiently elongated to allow sliding of the *sec*-butyl group over the aromatic ring to establish C(α)$^+$···C(3), C(*β*)-H···F, and C(*γ*)-H···F. The smaller activation enthalpy ($\Delta H^{\ddagger} = 8.9 \pm 0.6$ kcal mol^{-1}) and less favorable activation entropy ($\Delta S^{\ddagger} = -8.4 \pm 1.6$ cal mol^{-1} K^{-1}) measured for the competing **I** → **II** process (ii) reflect, instead, slightly tighter transition structures **C** and **D** in which the C(α)$^+$ center of the *sec*-butyl moiety still partially interacts with C(1) of fluorobenzene while moving over its C(2) and C(6) sites, respectively.

This mechanistic picture shows an analogy close to that proposed in our previous kinetic investigation on gas-phase isomerization of protonated $\mathbf{1^{Me}_S}$ (henceforth denoted as $\mathbf{I^{Me}}$).[23] In this study, only the *para* → *meta* isomerization was observed with complete racemization and partial H-scrambling in the moving *sec*-butyl moiety. The activation parameters of the isomerization without side-chain hydrogen scrambling ($\Delta H^{\ddagger} = 10.3 \pm 1.2$ kcal mol^{-1} and $\Delta S^{\ddagger} = -5.3 \pm 3.6$ cal mol^{-1} K^{-1}) are comparable with those measured for the analogous **I** → **II** and **I** → **IV** reactions. This suggests that the two sets of reactions proceed through similar transition structures characterized by extensive C(α)$^+$···C(1) elongation. The slightly smaller activation enthalpies and less favored activation entropies measured for the **I** → **II** and **I** → **IV** reactions likely reflect the effects of the second C(*γ*)-H···F interaction in the relevant transition structures (Figure 3) which is obviously absent in the reaction with $\mathbf{I^{Me}}$.

In addition to rotational transition structure **E** of Figure 3, the racemization of the *sec*-butyl moiety of **I** may simply involve a C(*β*) → C(α) hydrogen shift. The exploration of the relevant PES led to the location of the **F** transition structure for the 1,2-H shift (Figure 3) which is thought to connect the stable complexes **A** and **B′** (or **B″**). Compared to the **I** → **II** and **I** → **IV** processes (Table 3), both the competing **I** → **III** and **I** → **V** isomerizations (paths (iii) and (v) of Figure 4, respectively) are characterized by smaller activation enthalpies ($\Delta H^{\ddagger} = 6.9 \pm 0.9$ and 8.2 ± 1.0 kcal mol^{-1}, respectively) and much less favorable activation entropies ($\Delta S^{\ddagger} = -15.2 \pm 1.7$ and -11.3 ± 3.1 cal mol^{-1} K^{-1}, respectively). These findings are consistent with the tight transition structure **F**, wherein a C(*β*) → C(α) hydrogen shift participates in the C(α)$^+$···C(1) bond cleavage in **I**. This sort of hydride ion *anchimeric assistance* seems to be much less effective in the isomerization of $\mathbf{I^{Me}}$.[23] Indeed, the *para* → *meta* isomerization of $\mathbf{I^{Me}}$ involves activation parameters ($\Delta H^{\ddagger} = 16.9 \pm 3.1$ kcal mol^{-1} and $\Delta S^{\ddagger} = +9.9 \pm 7.0$ cal mol^{-1} K^{-1}) which suggest that the *sec*-butyl moiety undergoes a H-shift *only after the almost complete C(α)−C(1) bond cleavage*. This behavior may be explained by the hypothesis that a significant amount of positive charge must develop at the C(α) site of the *sec*-butyl moiety to promote the 1,2-H shift. This requirement can easily be fulfilled in **I** by the poor *π*-electron donating character of fluorobenzene (PA = 180.7 kcal mol^{-1})[33] which allows for the development of a sufficient amount of positive charge on

(44) Denhez, J. P.; Audier, H. E.; Berthomieu, D. *Org. Mass Spectrom.* **1993**, *28*, 704.
(45) Smith, W. B. *J. Phys. Org. Chem.* **2002**, *15*, 347 and references therein.

the C(α) center of the *sec*-butyl moiety, even in the presence of a substantial $C(\alpha)^+\cdots C(1)$ interaction. The same condition does not apply with $\mathbf{I^{Me}}$ whose aromatic moiety, i.e., toluene (PA = 187.4 kcal mol^{-1}),[33] is a better π-electron donor. In this case, an almost complete C(α)−C(1) bond cleavage is necessary to promote relocation of the positive charge from the ring to the C(α) center of the *sec*-butyl moiety.

Similar arguments apply to the **I** → **16** dealkylation reaction. According to Figure 4, the energy required for the unimolecular de-*sec*-butylation of **I** (23 kcal mol^{-1}) largely exceeds the activation enthalpy measured for the formation of fluorobenzene **16** from **I** ($\Delta H^{\ddagger} = 6.5 \pm 1.2$ kcal mol^{-1}). This discrepancy, coupled with the negative activation entropy value ($\Delta S^{\ddagger} = -12.0 \pm 3.6$ cal mol^{-1} K^{-1}), excludes any conceivable unimolecular **I** fragmentation to **16** while supporting the direct formation of fluorobenzene by the exothermic bimolecular β-elimination process induced by a $(C_2H_5)_3N$ attack at the side chain of **I** ($\Delta H_{elim} = -31$ kcal mol^{-1}).[33] The same base-induced elimination process on $\mathbf{I^{Me}}$ involves a larger activation energy ($\Delta H^{\ddagger} = 9.8 \pm 0.9$ kcal mol^{-1}) and a more favorable activation entropy ($\Delta S^{\ddagger} = -8.7 \pm 2.7$ cal mol^{-1} K^{-1}). This difference can be explained by the greater acidic character of the *sec*-butyl hydrogens of **I**, relative to those of $\mathbf{I^{Me}}$, which places the relevant base-induced elimination transition structure much earlier along the reaction coordinate.

Role of $\eta^{2'}$-Chelates in Gas-Phase Arene Alkylations. From the above experimental and computational results, it appears that the **I** isomerization is governed by a relatively flat PES region located more than 13 kcal mol^{-1} below the **I** → **16** + $sC_4H_9^+$ and **I** → **16**H^+ + 2-C_4H_8 dissociation limits and more than 8 kcal mol^{-1} below A&G's loosely bound π-complex (Figure 4). This low-energy region is characterized by the presence of several shallow potential energy wells corresponding to $\eta^{2'}$-chelates **A**, **B**, **B′**, and **B″** separated from the corresponding σ-bonded intermediates, **I**−**V**, by very limited energy barriers.[23,45,46] As suggested in a previous study,[23] these low-energy $\eta^{2'}$-chelates may play a crucial role in gas-phase aromatic alkylation reactions as well. The pronounced difference in the *ortho*/*meta* ratios arising from **I** isomerization (Table 1) and from the direct *sec*-butylation of fluorobenzene (Table 4), carried out under comparable experimental conditions, excludes the possibility that the first process proceeds through the same loosely bound π-complex proposed by A&G as an intermediate of the latter reaction.[19] Rather, such a difference is due to the different phase space experienced in the isomerization of **I** (or $\mathbf{I^{Me}}$) and in the gas-phase *sec*-butylation of fluorobenzene (or toluene). The first process necessarily proceeds through the initial exclusive formation of the corresponding **A**-type $\eta^{2'}$-complexes (Figure 4), whereas the latter involves the simultaneous (although not necessarily equal) population of all of the accessible isomeric $\eta^{2'}$-chelates from A&G's loosely bound π-complex. The product pattern from the **I** isomerization is the result of the extent of the one-way reaction pathways, (ii)−(v), from **A** before the quenching of the formed noncovalent transients into the corresponding σ-bonded intermediates. The product distribution from the *sec*-butylation of fluorobenzene reflects, instead, the interconversion among all of the simultaneously populated $\eta^{2'}$-complexes, before the relevant σ-bonding.

This model suitably accounts for the dramatic pressure dependence of the isomeric distribution of 2-arylbutanes from gas-phase arene *sec*-butylation (Table 4) at any given temperature. The limited extent of the proton-induced isomerization of $\mathbf{1^F_R}$ (Table 1) excludes facile interconversion among the corresponding isomeric σ-intermediates as a result of the observed pressure dependence. Indeed, at 70 Torr and 40−100 °C, the σ-bonded arenium ion **I** is found to be long-lived. Its limited isomerization rate constants (ca. 1×10^5 s^{-1} (at 40 °C) and ca. 9×10^5 s^{-1} (at 100 °C), Table 1) indicate that **I** undergoes from ca. 2000 (100 °C) to ca. 21400 (40 °C) collisions with CH_4 before rearranging to the *ortho* and *meta* isomers.[41] Thus, at 70 Torr and $T \leq 100$ °C, the **I** arenium ion lives long enough to be in thermal equilibrium with the bulk gas before reacting. The same conclusion is valid a fortiori when **I** and its regioisomers are generated under the same conditions by direct *sec*-butylation of fluorobenzene. Therefore, their relative population should depend only on the temperature and not on the bulk gas pressure. As a consequence, the large pressure effect on the isomeric distribution of products from gas-phase *sec*-butylation of fluorobenzene (Table 4) can be explained only by acknowledging the intermediacy of isomeric $\eta^{2'}$-type chelates with lifetimes comparable to their collision time with the bulk gas at 70−760 Torr ($2 \times 10^{-9} \div 2 \times 10^{-10}$ s).

The existence of relatively stable $\eta^{2'}$-chelates **B**, **B′**, and **B″** on the **I** PES accounts for the exceptional *ortho* selectivity exhibited by fluorobenzene in gas-phase alkylations.[24−26,38] At high gas pressures, when **B** undergoes several cooling collisions with the bulk gas, it tends to collapse preferentially to the *ortho* σ-bonded intermediate. At lower pressures, i.e., at lower cooling collision frequencies, the $\eta^{2'}$-complexes **B**−**B″** remain sufficiently hot to promote entropy-driven motions over the fluorobenzene ring (e.g., through the **E** transition structure) to allow the formation of other isomeric $\eta^{2'}$-type complexes (e.g., **A**) eventually collapsing to *para* and *meta* σ-bound intermediates, the latter being the thermodynamic sink of the entire process.

Acknowledgment. Financial support from the University of Rome "La Sapienza", the University Camerino, and the Italian National Research Council (CNR) is gratefully acknowledged. The authors express their gratitude to F. Grandinetti for his support in the theoretical calculations.

Supporting Information Available: Computational details for all of the structures shown in Figure 3 and for the *ipso*-protonated intermediates **I**−**V** of Scheme 3. This material is available free of charge via the Internet at http://pubs.acs.org.

JO050019Q

(46) Heidrich, D. *Angew. Chem., Int. Ed.* **2002**, *41*, 3208.